ResearchGate

See discussions, stats, and author profiles for this publication at: https://www.researchgate.net/publication/343783549

Nonlinear Optical Imaging, Precise Layer Thinning, and Phase Engineering in MoTe 2 with Femtosecond Laser

Article *in* ACS Nano · August 2020

DOI: 10.1021/acsnano.0c02649

CITATIONS
16

READS
299

6 authors, including:

Mengmeng Wang
University of Nebraska at Lincoln
31 PUBLICATIONS **809** CITATIONS
SEE PROFILE

Dawei Li
Dalian University of Technology
67 PUBLICATIONS **1,071** CITATIONS
SEE PROFILE

Kun Liu
Dalian University of Technology
121 PUBLICATIONS **1,091** CITATIONS
SEE PROFILE

Xin Li
Seoul National University
200 PUBLICATIONS **2,544** CITATIONS
SEE PROFILE

Some of the authors of this publication are also working on these related projects:

2D materials View project

Generation and transmission of a High-bit-rate optical millimeter wave View project

All content following this page was uploaded by Dawei Li on 27 August 2020.

The user has requested enhancement of the downloaded file.

ACSNANO

www.acsnano.org

ARTICLE

Nonlinear Optical Imaging, Precise Layer Thinning, and Phase Engineering in $MoTe_2$ with Femtosecond Laser

Mengmeng Wang, Dawei Li,* Kun Liu, Qitong Guo, Sumei Wang, and Xin Li

Cite This: https://dx.doi.org/10.1021/acsnano.0c02649

Read Online

ACCESS | Metrics & More | Article Recommendations | Supporting Information

ABSTRACT: The control of layer thickness and phase structure in two-dimensional transition metal dichalcogenides (2D TMDCs) like $MoTe_2$ has recently gained much attention due to their broad applications in nanoelectronics and nanophotonics. Continuous-wave laser-based thermal treatment has been demonstrated to realize layer thinning and phase engineering in $MoTe_2$, but requires long heating time and is largely influenced by the thermal dissipation of the substrate. The ultrafast laser produces a different response but is yet to be explored. In this work, we report the nonlinear optical interactions between $MoTe_2$ crystals and femtosecond (fs) laser, where we have realized the nonlinear optical characterization, precise layer thinning, and phase transition in $MoTe_2$ using a single fs laser platform. By using the fs laser with a low fluence as an excitation light source, we observe the strong nonlinear optical signals of second-harmonic generation and four-wave mixing in $MoTe_2$, which can be used to identify the odd−even layers and layer numbers, respectively. With increasing the laser fluence to the ablation threshold (F_{th}), we achieve layer-by-layer removal of $MoTe_2$, while 2H-to-1T′ phase transition occurs with a higher laser fluence ($2F_{th}$ to $3F_{th}$). Moreover, we obtain highly ordered subwavelength nanoripples on both the thick and few-layer $MoTe_2$ with a controlled fluence, which can be attributed to the fs laser-induced reorganization of the molten plasma. Our study provides a simple and efficient ultrafast laser-based approach capable of characterizing the structures and modifying the physical properties of 2D TMDCs.

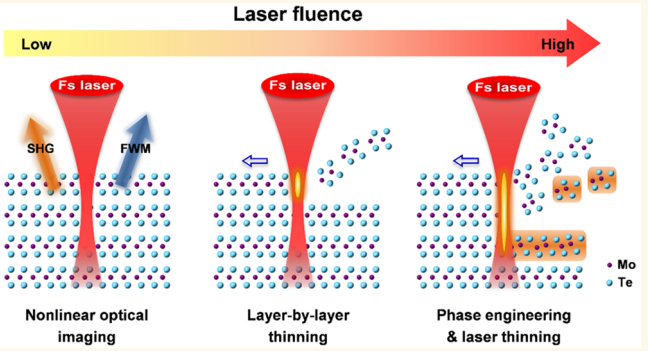

KEYWORDS: *$MoTe_2$, femtosecond laser, nonlinear optical response, phase transition, layer thinning, laser-induced periodic nanostructures*

Downloaded via Dawei Li on August 27, 2020 at 21:41:52 (UTC).
See https://pubs.acs.org/sharingguidelines for options on how to legitimately share published articles.

Two-dimensional transition metal dichalcogenides (2D TMDCs) have gained extensive attention due to their diverse structure and excellent optical and electronic properties.[1−4] For example, the inversion asymmetry and strong spin−orbital coupling in TMDCs may induce the valley-polarized emission, which leads to the emergence of valleytronics.[3] The strong nonlinear optical (NLO) responses in TMDCs advance potential applications in 2D photonic and optoelectronic devices.[4−6] Recently, molybdenum ditelluride ($MoTe_2$) has arisen as an appealing TMDC because it can be easily phase engineered, due to its extremely small energy difference ΔE between semiconducting 2H phase and semimetallic 1T′ phase (ΔE < 50 meV).[7] Laser irradiations,[8,9] strain engineering,[10−12] hydrogen plasma etching,[13] ozone treatment,[14] electrostatic doping,[15] and controlled chemical vapor deposition (CVD)[7,16−18] have been employed to achieve phase transition in $MoTe_2$ crystals. Among these methods, continuous-wave (CW) laser irradiation is considered as a direct and clean approach to realize both layer control and phase engineering by heating and evaporating the $MoTe_2$ on top layers.[8,9,19] However, a long irradiation time of heating up 2D layers may cause residual stress in crystals after cooling. Besides, the CW laser processing parameters used are highly dependent on the thermal conductivity of the substrate.[19]

As mentioned above, the CW-laser treatment is dominated by the thermal effect, which requires accumulated heating time to affect the lattice structure.[20] Differently, an ultrafast laser pulse has a strong peak power, which enables the processing of a lattice structure within very short time scales and the heat affected zone was reduced.[21−24] Previously, ultrafast lasers with

Received: March 29, 2020
Accepted: August 20, 2020
Published: August 20, 2020

© XXXX American Chemical Society

a pulse duration of tens of femtoseconds (fs) were applied to remove graphene layer-by-layer through raster scanning the top surfaces.[25,26] In addition, the fs laser has been utilized to exfoliate TMDCs in solutions.[27] These studies have demonstrated the feasibility of an ultrafast laser as a powerful tool to realize layer thinning and exfoliation, while the possibility of achieving phase transition and periodic nanostructures in 2D TMDCs, especially for $MoTe_2$ crystals, using fs laser irradiation is yet to be explored. Recently, it has been reported that the spontaneous periodic micro/nanostructures can be generated in bulk or thick MoS_2 crystals by a fs laser.[28,29] However, it remains unclear whether the laser-induced periodic surface structure (LIPSS) formation, a universal phenomenon during ultrafast laser ablation in normal bulk materials,[30] can occur in the atomically thin 2D materials.

In this work, we report the interactions between the exfoliated $MoTe_2$ flakes and the fs laser (Figure 1), where

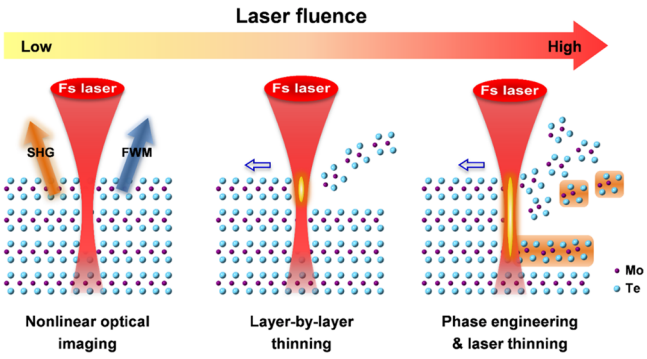

Figure 1. Schematic view showing different interactions between $MoTe_2$ layers and fs laser by varying the laser fluence: nonlinear optical characterization (left panel), precise layer thinning with no phase change (middle panel), and phase engineering and laser thinning (right panel).

the nonlinear optical imaging, precise laser thinning, and phase engineering in $MoTe_2$ have been realized by controlling the fs laser fluence. By using the fs laser at a low fluence as the excitation light source, we investigated the NLO properties of $MoTe_2$ and established the relationship between the second-order and third-order NLO signals and 2D layer numbers. With increasing the laser fluence to the ablation threshold (F_{th}), a single-layer thinning in $MoTe_2$ has been achieved, while 2H-to-1T′ phase transition in $MoTe_2$ occurs by fs laser irradiation with a high fluence ranging from $2F_{th}$ to $3F_{th}$. More interestingly, we find that fs laser irradiation with a high fluence can be applied to generate highly ordered nanoripple structures in $MoTe_2$ thin films. Our work demonstrates the versatility of the ultrafast laser in optical characterization, phase engineering, and nanomanufacturing, pointing to an easy and efficient strategy for functional design of 2D nanoelectronic and nanophotonic devices.

RESULTS AND DISCUSSION

Nonlinear Optical Responses in $MoTe_2$. Two-dimensional layered TMDCs such as MoS_2 and ReS_2 have been shown to exhibit strong nonlinear optical responses under the intense ultrafast laser irradiation without damaging the sample [*e.g.*, second-harmonic generation (SHG),[31,32] third-harmonic generation (THG),[33] and four-wave mixing (FWM)[6]]. Very recently, researchers have observed strong SHG in 2H-$MoTe_2$ with odd numbers of layers[34] and 1T′-$MoTe_2$ with even numbers of layers,[35] both owing to the broken inversion symmetry.[15] So far, other nonlinear optical properties of $MoTe_2$ have not been studied (Figure 2a). Here, few-layer and thick flakes of $MoTe_2$ were exfoliated from bulk crystals, and the layer numbers were determined by optical microscopy and atomic force microscopy (AFM). Figure 2b shows the optical image of a $MoTe_2$ flake transferred on a silicon substrate with layer numbers ranging from bilayer (2L) to eight layers (8L). The phase structure of $MoTe_2$ was identified using Raman spectroscopy (Figure 2b inset). The presence of two characteristic Raman peaks at 174 cm^{-1} (out-of-plane A_{1g} mode) and 235 cm^{-1} (in-plane E^1_{2g} mode) confirms the 2H phase crystalline structure. Next, we used multiphoton nonlinear optical microscopy to detect the nonlinear optical responses of 2H $MoTe_2$ by focusing the pump (ω_1)−probe (ω_2) laser beams with a low fluence of about 9 mJ/cm^2 onto the sample. It should be noted that the entire fs laser experiments were conducted in air (see Methods). We observed two strong peaks from the nonlinear optical spectrum in a 3L $MoTe_2$ (not shown): one is at about 400 nm and the other is at about 650 nm. The peak frequency at 400 nm is equal to $2\omega_1$ and the peak signal at 650 nm is equal to $2\omega_1 - \omega_2$, indicating that these two peak signals are originated from SHG and FWM processes, respectively. We also performed the laser power dependent SHG study of a 3L $MoTe_2$ (Figure 2c inset), further confirming its intrinsic second-order nonlinear character.

Figure 2c and d display the SHG and FWM imaging of the same sample in Figure 2b. It can be seen in Figure 2c that the SHG signal for odd-layer 2H-$MoTe_2$ is much stronger than that with even numbers of layers. Theoretically, the SHG signal only appears at odd-numbered layers with inversion asymmetry, but is negligible at even-numbered layers.[36] In our case, the presence of a weak SHG signal in even layers is probably caused by the local dielectric environment and the enhanced susceptibility due to the increased density of electronic state at the Γ point.[37] The layer number dependent SHG measurement (Figure 2e) shows that the signal gradually decreases for odd-layer $MoTe_2$ (blue curve), while there is a slight SHG signal increase for even-layer $MoTe_2$ (red curve). However, different behaviors were observed by Song *et al.*, who reported that the SHG signal in odd-layered 2H-$MoTe_2$ increases (decreases) with layer numbers less than (more than) five, which was attributed to the optical absorption of the SHG signal by $MoTe_2$.[34] In our case, the attenuation of the SHG signal for odd-layer $MoTe_2$ can be explained by the wave propagation effect and absorption effect of the fundamental and SH fields.[31] We also performed the SHG measurements on other TMDCs like MoS_2 for comparison (Figure S1c, Supporting Information). The results show that the SHG behavior in $MoTe_2$ and MoS_2 obeys the same layer number dependence. For a fixed layer number, the SHG intensity of $MoTe_2$ is comparable with that of MoS_2. Figure 2f shows the FWM intensity as a function of $MoTe_2$ layer thickness, clearly exhibiting a linear relationship. This observation is similar to the behavior of FWM in other 2D materials, such as MoS_2[6] and graphene,[38] which can be explained by the constructive interference of radiated fields from different layers.[38] Figure S1d compares the FWM response between $MoTe_2$ and MoS_2. The FWM intensity in $MoTe_2$ is stronger, which is about 4 times that in MoS_2 with the same layer number. Overall, 2D $MoTe_2$ as a nonlinear photonic crystal shows the great

https://dx.doi.org/10.1021/acsnano.0c02649
ACS Nano XXXX, XXX, XXX−XXX

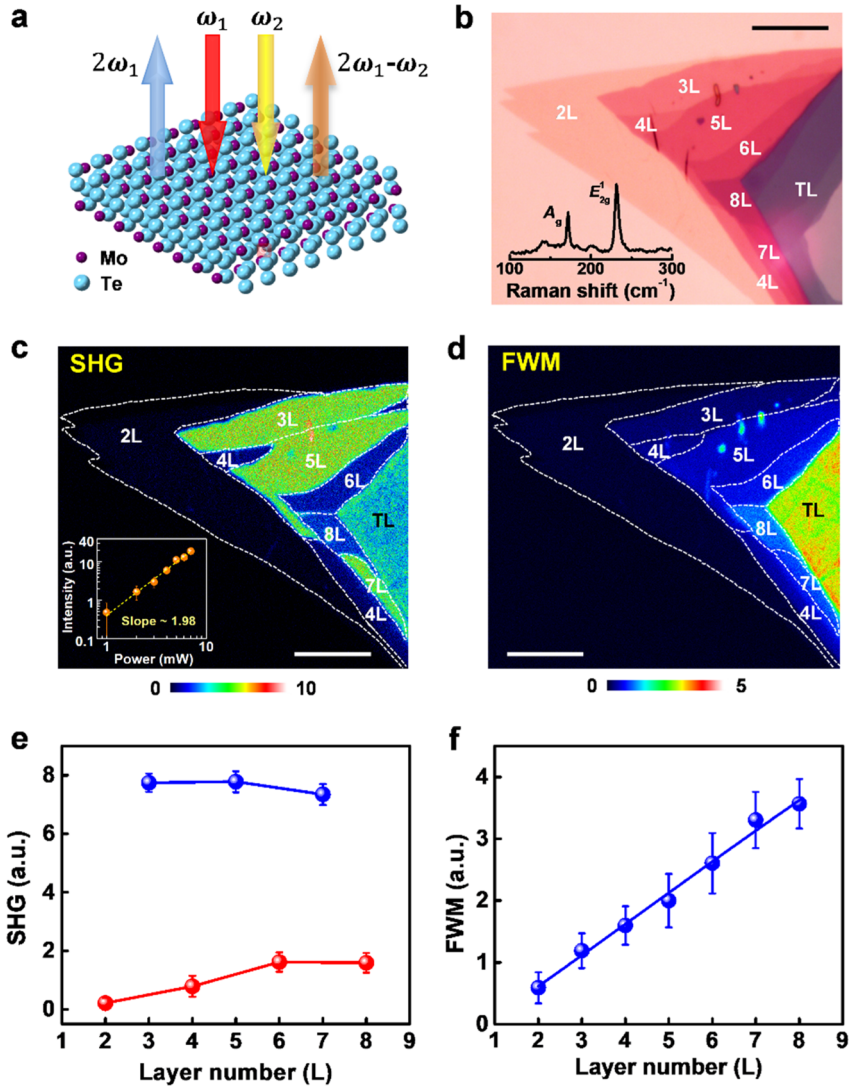

Figure 2. Nonlinear optical imaging characterization. (a) Schematic of the multiphoton nonlinear optical responses in $MoTe_2$. (b) Optical image, (c) SHG mapping, and (d) FWM mapping of an exfoliated $MoTe_2$ sample with different layer numbers. The excitation fs laser fluence is 9 mJ/cm^2. Inset in (b): Raman spectrum of a $MoTe_2$, showing a 2H-phase crystal structure. Inset in (c): SHG intensity of a 3L $MoTe_2$ as a function of excitation laser power. The scale bars in (b)−(d) are 10 μm. (e) SHG and (f) FWM intensity as a function of $MoTe_2$ layer number.

potential for NLO applications,[39,40] such as frequency converters.

Layer Thinning and Phase Engineering in Thick $MoTe_2$. A thick flake of $MoTe_2$ (~18 nm) transferred on a silicon substrate (Figure S2, Supporting Information) was employed to investigate the morphological control and phase transition with fs laser irradiation. An ablation threshold F_{th} of 18.4 mJ/cm^2 was confirmed, where F_{th} is defined as the minimum energy required to remove one layer from the $MoTe_2$ top surfaces. Figure 3a shows the layer thinning results through scanning a square of 10 × 10 μm^2 by a fs laser at a fluence of F_{th} for one and three scans. Note that one scanning process takes about 35 s, corresponding to a scanning rate of ~3 μm^2/s, which is much faster than the previously reported values *via* CW-laser treatment.[8,9,19] The thickness decrease for one scan is around 1 nm (upper panel, Figure 3b), which is close to the monolayer thickness of $MoTe_2$ (~0.7 nm),[41] indicating a single layer thinning from 2D surfaces. The thickness decrease after three scans is nearly 3 times of that of one scan (lower panel, Figure 3b), revealing a linear relationship between the thickness decrease and the scan times. The ablated areas after fs laser thinning have a surface roughness of about 0.67 and 0.60 nm, respectively, for one and three scans (Figure 3c and Figure S3a, Supporting Information). The phase structure of $MoTe_2$ before and after fs laser thinning was investigated *via* Raman measurement. The thinned areas only feature the A_g and E^1_{2g} peaks of 2H-$MoTe_2$ (Figure 3d and Figure S4, Supporting Information), consistent with the pristine layers. Thus, layer-by-layer thinning without phase transition or oxidation is achieved with a relatively low fs laser fluence of F_{th}.

Figure 4a shows an optical image of the same $MoTe_2$ sample in Figure S2 after scanning by a fs laser at higher fluences of $2F_{th}$ (upper) and $3F_{th}$ (lower) for one and three scans. The squares for three scans are smoother than those scanned once, as confirmed by surface roughness statistics (Figure S3a−c, Supporting Information), indicating the smoothing effect with more fs laser scans. In addition, we find that the thickness

https://dx.doi.org/10.1021/acsnano.0c02649
ACS Nano XXXX, XXX, XXX−XXX

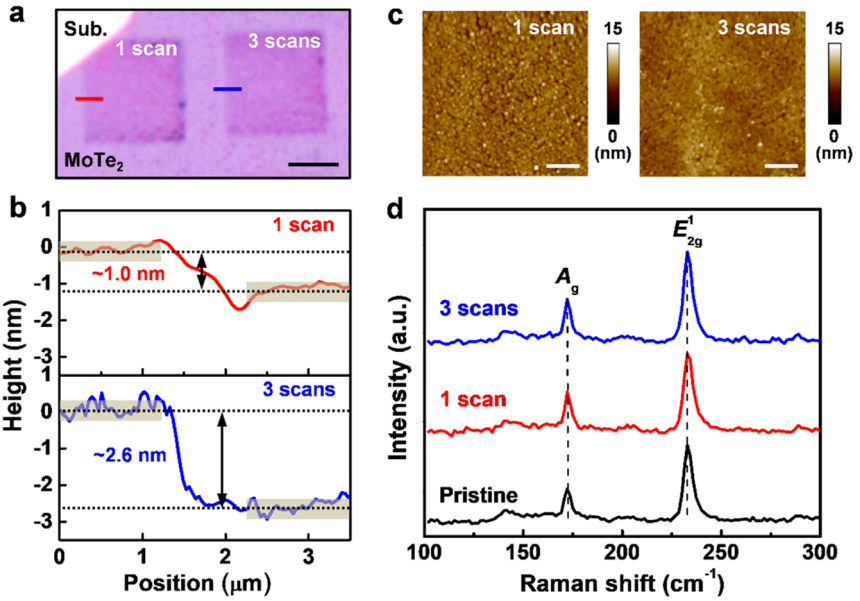

Figure 3. Layer-by-layer thinning in thick $MoTe_2$ with a fs laser. (a) Optical image of a thick flake of $MoTe_2$ (~18 nm) after fs laser scanning with a fluence of 18.4 mJ/cm^2 (F_{th}, ablation threshold) for one time (left square region) and three times (right square region). The scale bar is 5 μm. (b) Corresponding thickness profiles along the red and blue lines in (a). (c) AFM topography images of ablated areas in (a) after one scan (left panel) and three scans (right panel). The scale bars are 200 nm. (d) Raman spectra of the pristine $MoTe_2$ (black) and $MoTe_2$ after irradiation with F_{th} for one scan (red) and three scans (blue).

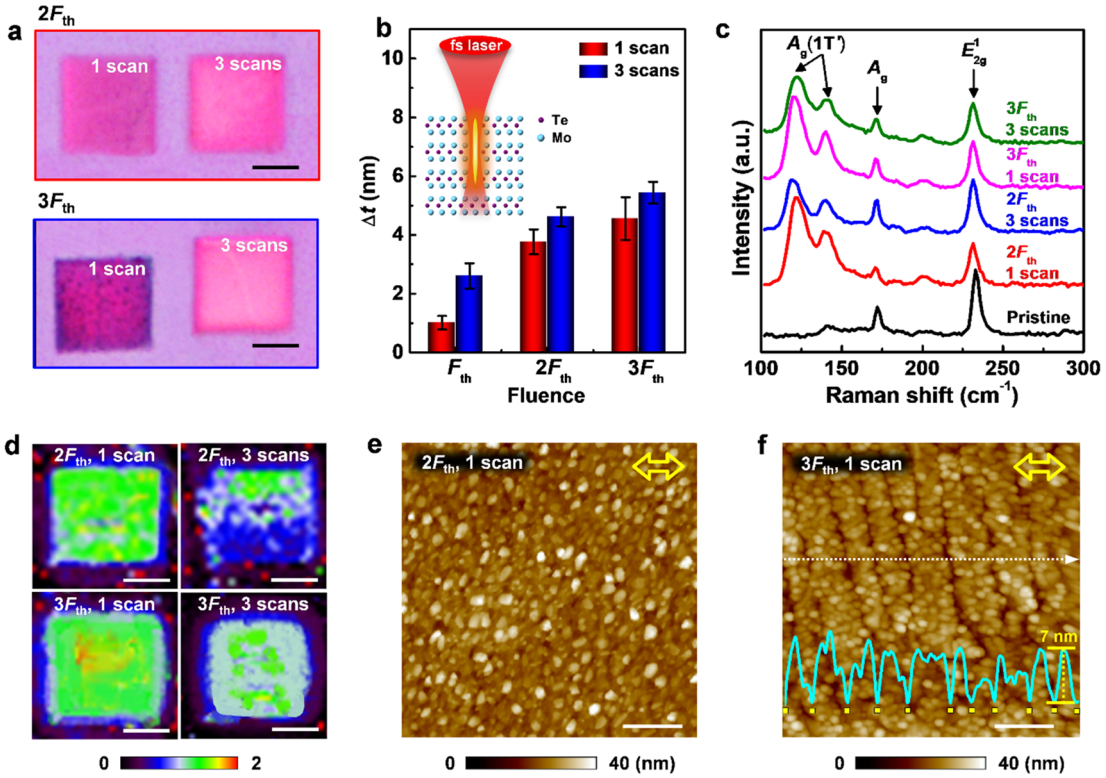

Figure 4. Phase engineering in thick $MoTe_2$ with a fs laser. (a) Optical image of a thick flake of $MoTe_2$ (~18 nm) after fs laser irradiation with fluences of $2F_{th}$ (upper panel) and $3F_{th}$ (lower panel) for one and three scans. The scale bars are 5 μm. (b) Thickness decrease (Δt) of $MoTe_2$ as a function of fs laser fluence. Inset: Schematic showing the interaction between $MoTe_2$ and fs laser. (c) Typical Raman spectra of thick $MoTe_2$ after fs laser irradiation with fluences of $2F_{th}$ and $3F_{th}$ for different scans. (d) Raman mapping of the intensity ratio of $A_{1g}(1T')/E^1_{2g}$ for the same sample in (a). The scale bars are 5 μm. (e, f) AFM topography images of the irradiated $MoTe_2$ with a laser fluence of (e) $2F_{th}$ and (f) $3F_{th}$ for one scan. The scale bars are 200 nm. The yellow arrows mark the fs laser polarization. Inset in (f) shows the height profile along the white dotted line.

decrease at a high fluence of $2F_{th}$ or $3F_{th}$ (~4 nm or ~5 nm) for one scan is much larger than that with a fluence of F_{th} (~1 nm), which can be explained by the effectively affected thickness (EAT, see yellow region in Figure 4b inset). In our

https://dx.doi.org/10.1021/acsnano.0c02649
ACS Nano XXXX, XXX, XXX−XXX

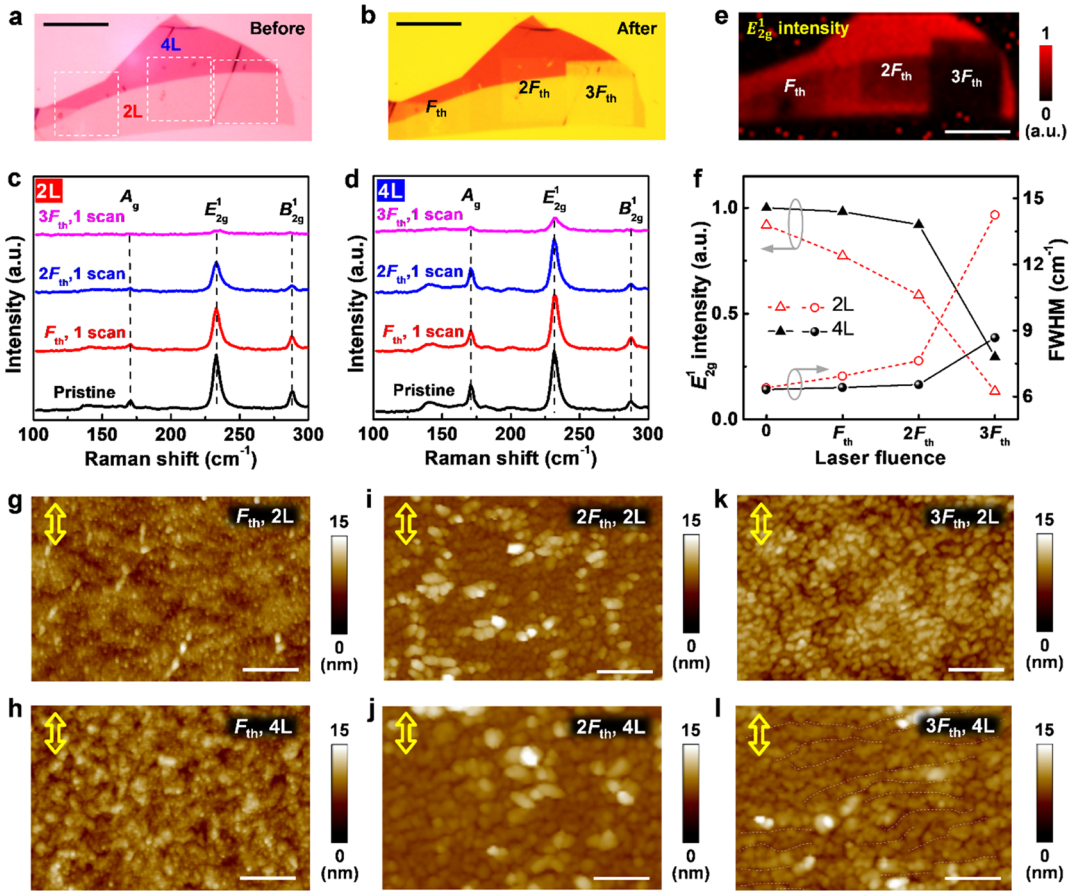

Figure 5. Effect of fs laser fluence on atomically thin $MoTe_2$. (a, b) Optical images of a few-layer $MoTe_2$ sample consisting of a 4L region (top) and a 2L regions (bottom) (a) before and (b) after irradiation by a fs laser with fluences of F_{th} (left square), $2F_{th}$ (middle square), and $3F_{th}$ (right square). (c, d) Raman spectra of (c) 2L and (d) 4L $MoTe_2$ after fs laser irradiation with different fluences. (e) E^1_{2g} intensity mapping for the same sample in (b). (f) E^1_{2g} peak intensity and fwhm in 2L and 4L $MoTe_2$ as a function of fs laser fluence. (g–l) AFM topography images of the (g, i, k) 2L region and (h, j, l) 4L region after fs laser irradiation with a fluence of F_{th} (g, h), $2F_{th}$ (i, j), and $3F_{th}$ (k, l). The yellow arrows in (g)–(l) mark the fs laser polarization. The scale bars are 10 μm in (a), (b), and (e) and 200 nm in (g)–(l).

experiment, the Rayleigh length (Z_R) of the focused laser beam (~3.4 μm, see Methods) for a given spot size is much larger than the $MoTe_2$ thickness (~18 nm). Therefore, the laser fluence varies less than 0.01% when propagating along the whole depth of 2D layers, and the EAT is mainly determined by the absorption of the $MoTe_2$ layers. When the propagation distance is 2 orders of magnitude smaller than Z_R, the attenuated laser fluence (F) can be estimated using the Beer–Lambert law:[42]

$$F = F_0 e^{-\alpha T} \quad (1)$$

where F_0, α, and T are the initial laser fluence, the absorption coefficient (0.2 nm^{-1} for the laser wavelength centered at 800 nm[43]), and the EAT, respectively. Considering the attenuated fluence passing through one layer is just high enough for layer removal under the laser fluence of F_{th}, we obtained

$$F_{th} e^{-\alpha(T_1)} \approx 2F_{th} e^{-\alpha(T_2)} \approx 3F_{th} e^{-\alpha(T_3)} \quad (2)$$

Given $T_1 \approx 0.7$ nm for single layer removal, we extracted the value of $T_2 \approx 4$ nm and $T_3 \approx 6$ nm for the fluence of $2F_{th}$ and $3F_{th}$, respectively, which is in good agreement with our experimental observation for one scan. Additionally, the thickness decrease with a high fluence ($2F_{th}$ or $3F_{th}$) for three scans is only about 1 nm larger than that for one scan (Figure 4b). This observation is clearly different from the linear scan–depth relationship at a low fluence of F_{th}, which can be explained by the fs laser-induced surface scattering effect. The initial scan at a higher laser fluence has a "plowing" effect, to remove certain thickness and form nanostructures on $MoTe_2$ top layers, while the subsequent scans mainly ablate those nanostructures on top surfaces due to the scattered laser light, thereby leading to the reduced ablation depth with more scans.

Next, we carried out Raman studies on the ablation areas to monitor the phase change in thick $MoTe_2$ (Figure 4c). We observed similar Raman spectra with $2F_{th}$–$3F_{th}$ for one and three scans. Except for the Raman peaks from the 2H phase, two new Raman peaks at 124 and 138 cm^{-1} originating from the A_g band of 1T′ phase appear. The phase transition from 2H to 1T′ $MoTe_2$ under fs laser irradiation can be explained by the electronic excitation that results in a structural symmetry breaking.[44−46] This phase transition occurs within sub-picosecond time scales,[44] much shorter than that of accumulated heat by a CW laser for phase transition.[8,9] The coexistence of 1T′ and 2H phases reveals that the top layers have been changed to the 1T′ phase, while the bottom layers remain the 2H phase, leading to a vertical homojunction.[8] A fs laser-induced 1T′/2H heterostructure is helpful for studying the interfacial properties of a $MoTe_2$ homojunction and the ferroelectric properties of 1T′-phase $MoTe_2$ on top.[17,47] The

https://dx.doi.org/10.1021/acsnano.0c02649
ACS Nano XXXX, XXX, XXX–XXX

analysis of the full width at half-maximum (fwhm) for the E^1_{2g} peak of 2H phase layers (Figure S3d, Supporting Information) reveals that defects were produced in thick $MoTe_2$ after fs laser irradiation, which increases with the laser fluence. Interestingly, no oxides, such as TeO_2, MoO_2, and MoO_3, are detected in either top 1T′ or bottom 2H layers (Figure S4, Supporting Information). Raman mapping of the intensity ratio of $A_g(1T')$ at 124 cm^{-1} to E^1_{2g} at 235 cm^{-1} was performed to confirm the uniform distribution as well as the degree of phase transition in the fs laser irradiated area (Figure 4d). The $A_g(1T')/E^1_{2g}$ peak intensity ratios with the fluences of $2F_{th}$ and $3F_{th}$ for one scan are similar (~1.5), which is higher than that with three scans (~1).

Moreover, we investigated the surface topographies of the irradiated area (Figure 4e and f). Different from the randomly nanoparticle structures formed on $MoTe_2$ surfaces with a laser fluence of $2F_{th}$ (Figure 4e), we clearly see highly ordered nanoripple structures on the irradiated area at $3F_{th}$ after one scan (Figure 4f and Figure S5a, Supporting Information). This suggests that the nanostructure formation is very sensitive to the laser fluence. The nanoripples represent a period (R) of about 100 nm and a depth (D) of about 7 nm, corresponding to a low aspect ratio (D/R) of 0.07. These ripple structures are well aligned along the direction perpendicular to the incident laser polarization (yellow arrows). This kind of nanostructure is called high-spatial-frequency LIPSS, which is frequently discovered in the fs-laser-processed bulk materials.[48] Researchers have proposed several formation mechanisms for LIPSS, such as self-organization,[49] twinning,[50] and plasmonic effects,[51] which, however, remain in debate. In our case, we proposed a three-stage model to explain the nanoripple formation in 2D $MoTe_2$. During the fs laser irradiation of $MoTe_2$ layers, the energy of the fs pulse is first absorbed by the electrons from 2D layers within a pulse duration and then transferred to the 2D lattices by electron−phonon relaxation (stage I). The 2D lattices are heated to the melting point (normally several picoseconds), followed by the molten plasma expansion and nanoparticle ejection (stage II). After material ejection, the 2D lattices are rapidly cooled. During the cooling process, the reorganization of the molten plasma takes place, which is attributed to the surface erosion and atomic diffusion effects,[48] thereby leading to nanoripple formation in 2D layers (normally several microseconds) (stage III).[21,22] It should be noted that the lasting time of fs laser-induced high temperature for nanoripple formation is much shorter than the accumulated heating time by a CW laser to affect the lattice structure.

Effect of fs Laser Fluence on Atomically Thin $MoTe_2$. As discussed above, we have realized layer thinning, phase engineering, and nanoripple formation in thick flakes of $MoTe_2$ with controlled fs laser fluences. Can a similar tailoring effects occur in the atomically thin $MoTe_2$? To answer this question, we prepared a few-layer $MoTe_2$ sample *via* mechanical exfoliation from its bulk crystals and then transferring it to a silicon substrate (Figure 5a). The layer numbers were determined using optical microscopy and AFM measurements. The few-layer $MoTe_2$ flake in Figure 5a consists of two parts: a four-layer (4L) region (upper) and a bilayer (2L) region (lower). The black curves in Figure 5c and d show the Raman spectra for pristine 2L and 4L, where a strong out-of-plane B^1_{2g} model at 289 cm^{-1} is observed. By examining the peak intensity ratio of B^1_{2g} to E^1_{2g}, the number of layers of $MoTe_2$ was further confirmed.[41]

Figure 5b shows optical image of the same sample in Figure 5a after scanning once with fs laser fluences of F_{th} (left square), $2F_{th}$ (middle square), and $3F_{th}$ (right square). Different optical contrasts observed in three irradiated areas suggest different thickness change by varying the fs laser fluence. A slight change in optical contrast is observed in both 2L and 4L regions with F_{th} and $2F_{th}$. As the laser fluence is increased to $3F_{th}$, the thickness of the 4L region obviously becomes thinner. Now the optical contrast of 4L is very close to that of pristine 2L, which indicates that 4L has been thinned to 2L. The similar layer thinning behavior occurs in the 2L region. According to the optical contrast, 2L is thinned to be a monolayer after $3F_{th}$ laser irradiation. Note that the laser fluence required for layer thinning of few-layer $MoTe_2$ (~$3F_{th}$) is much higher than that for a thick flake (~F_{th}), revealing a strong thickness-dependent ablation threshold for layer thinning of layered structures.[52]

We next performed the Raman studies of few-layer $MoTe_2$ with different fs laser fluences. Figure 5c−e show that all Raman peaks of the pristine 2L and 4L $MoTe_2$ are slightly decreased with F_{th} and $2F_{th}$ laser irradiation, but significantly decreased with a higher fluence of $3F_{th}$. It has been reported that the Raman intensity is proportional to the layer thickness of few-layer $MoTe_2$.[53] Thus, the nonlinear decrement of E^1_{2g} peak intensity with laser fluence (Figure 5f, left-axis plot) indicates that the layer removal (or thinning) highly depends on the laser fluence, consistent with our optical contrast analysis. We observed the weak Raman signal in the 2L region even after laser irradiation with a high fluence of $3F_{th}$. This further confirms that an ultrathin $MoTe_2$ layer remains on the substrate. Different from that occurring in the thick flake, no Raman peaks of the 1T′ phase appear in the few-layer sample after $2F_{th}$ and $3F_{th}$ laser irradiation (Figure 5c and d). This suggests that only layer thinning but no phase transition has been achieved in the few-layer $MoTe_2$ with a laser fluence of no more than $3F_{th}$.

As mentioned above, there is a laser threshold that is required for layer thinning (TH_{LT}) in $MoTe_2$. It is reasonable to deduce that there also exists a laser threshold for phase transition (TH_{PT}) in $MoTe_2$. For thick-layer $MoTe_2$, the value of TH_{PT} is about $2F_{th}$, higher than the value of TH_{LT} (~F_{th}). A similar rule may be applied for the few-layer $MoTe_2$. The value of TH_{LT} is increased to ~$3F_{th}$ for few-layer $MoTe_2$. Thus, it can be predicted that the value of TH_{PT} for few-layer $MoTe_2$ should be higher than $3F_{th}$. This explains why no phase change occurs in few-layer $MoTe_2$ with a fluence of $3F_{th}$. The strong layer thickness dependence of TH_{PT} and TH_{LT} can be attributed to the varying band gap[54] and/or nonlinear optical absorption[36] with layer numbers. The fs laser-induced phase transition process in $MoTe_2$ is accompanied with layer thinning. Assuming we use a fs laser fluence that is higher than its TH_{PT}, it is possible that the layer thinning is dominated in the few-layer $MoTe_2$. This means that most of the $MoTe_2$ layers could be thinned (or ablated) during the phase transition, thus making it difficult to realize the phase transition in a few-layer sample.

Figure 5f (right-axis plot) shows the fwhm of the E^1_{2g} peak as a function of laser fluence. The fwhm is slightly increased after irradiation with a fluence of F_{th} and $2F_{th}$, which suggests that the crystallinity is preserved and a few defects on the top layer start to appear. A sharp increase in fwhm with a fluence of $3F_{th}$ clearly demonstrates that more defects are generated in $MoTe_2$. The fs laser-induced defects and layer thinning in few-layer $MoTe_2$ could be correlated to its nonlinear optical

https://dx.doi.org/10.1021/acsnano.0c02649
ACS Nano XXXX, XXX, XXX−XXX

responses (Figure S6, Supporting Information). Figure S6a shows the SHG mapping for the same sample in Figure 5b. After laser irradiation with fluences of F_{th} and $2F_{th}$, an enhanced SHG signal is observed at some local areas from both 2L and 4L regions. This reveals that some defects have been created on 2L and 4L top layers, resulting in crystal symmetry breaking. The SHG enhancement is more obvious at the square boundaries (see white arrows in Figure S6a), which is due to the velocity decrease of the galvanometer scanner during steering back, leading to laser ablation of more $MoTe_2$ top layers. With increasing the laser fluence to $3F_{th}$, the SHG signal of the 4L area is strongly suppressed, similar to that of the pristine 2L area. This indicates that a two-layer thinning is completed, consistent with optical observation in Figure 5b. In contrast, the SHG signal of the 2L area after $3F_{th}$ laser irradiation becomes stronger than that without processing. In combination with the optical and Raman analyses above, it can be concluded that we have obtained 1L $MoTe_2$ *via* fs laser thinning. Figure S6b shows the FWM mapping for the few-layer $MoTe_2$ in Figure 5b. It is clear that the FWM signal is sensitive to the layer thickness change but not the defects. Overall, the intrinsic nonlinear optical characteristics of $MoTe_2$ have been proved to be an efficient way to identify the defect distribution and monitor the layer thinning process, *etc.*

Finally, we analyzed the evolution of surface morphologies in few-layer $MoTe_2$ by varying the fs laser fluence. As shown in Figure 5g and h, both 2L and 4L areas are still continuous after a fs laser scan once with a fluence of F_{th}. When increasing the laser fluence to $2F_{th}$, discontinuous but well aligned nanoripples are formed on the 2L area (Figure 5i), while the nanoripple structure is not obvious on the 4L area (Figure 5j). The discontinuous ripples are perpendicular to the incident laser polarization (yellow arrows), suggesting a similar formation mechanism to nanoripples generated on the thick flake. Figure 5k displays an AFM topography image of 2L $MoTe_2$ after irradiation with a laser fluence of $3F_{th}$, which shows that the material is ablated into the randomly distributed nanosheets. In the 4L region (Figure 5l), we observed discontinuous but relatively long nanoripples (marked by white dotted lines), possessing the same orientation as those in Figure 5i. Although well-ordered nanoripples can be achieved in atomically thin 2D materials, future work will be focused on the improvement of nanoripple quality and uniformity by optimizing the fs laser processing parameters, including scan speed, laser wavelength, pulse duration, environment, *etc.*[44,55] These parameters are also expected to have important influence on the phase transition and layer thinning of 2D TMDCs.

CONCLUSIONS

In summary, we have realized fast optical characterization, laser-by-layer thinning, and phase engineering in $MoTe_2$ by a fs laser with controlled fluences in a single platform. We also have achieved laser-induced highly ordered subwavelength (~100 nm) nanoripple structures on both thick and few-layer $MoTe_2$. Our work provides an efficient integration platform for the simultaneous optical characterization, phase engineering, and nanomanufacturing of 2D TMDCs. It is expected that this strategy could be applied to other van der Waals materials, providing an alternative approach to the design of high-performance nanoelectronic and nonlinear nanophotonic devices based on 2D materials.

METHODS

Sample Preparation. 2H-$MoTe_2$ flakes with different layer thicknesses were fabricated by mechanical exfoliation from the bulk single crystals (2D Semiconductors Inc.) using double-sided Scotch tape and then transferred to the silicon substrates by a dry transfer technique. The layer thickness of the sample was characterized by combined optical microscopy, atomic force microscopy, and Raman spectroscopy.

Nonlinear Optical Characterizations. A fs laser with a center wavelength of 800 nm, a pulse duration of 50 fs, and a repetition of 80 MHz was used as the irradiation source. The output beam was split into two parts, where one passing a combination of a half wave plate and a polarizer acted as the pump source and the other passed a 12 cm photonic-crystal fiber to generate a white light continuum (WLC) with a spectral range of 820−1100 nm, serving as the probe source. The pump and probe beams were collinearly focused on the sample surfaces by a water immersed objective (1.05 NA, 25×, 2 mm WD) (Figure S7, Supporting Information). To avoid water contact, we placed a 0.17 mm thick glass cover on top of the sample, which forms a thin air gap of ~0.06 mm between $MoTe_2$ and the glass cover. The spot size (w_0 = 1.22 λ/NA) of the focused laser beam is about 0.93 μm in radius, and the Rayleigh length ($Z_R = \pi w_0^2/\lambda$) is about 3.4 μm. The nonlinear optical mapping was realized by scanning the beam with a galvanometer scanner. The SHG and FWM nonlinear optical signals were collected by two PMTs with different filters inserted. The SHG signal was generated by the pump laser with a wavelength of 800 nm, where the filter used was 400 ± 10 nm. The FWM signal was generated through the 800 nm pump and the WLC probe, where the filter of 650 ± 40 nm was used. We used the same fs laser for nonlinear optical characterization and $MoTe_2$ processing (*i.e.*, layer thinning and phase engineering). The scanning speed for fs laser processing was fixed at 480 μm/s, and the line pitch was fixed at 6 nm.

Other Characterizations. Raman measurements were carried out in a micro Raman system (Renishaw InVia Plus) using a 514 nm laser with a power of 5 mW as the excitation source. The Raman spectra were collected with a 50× objective, with an accumulation time of 2 s. An AFM (Agilent 5500, CA) system running in tapping mode was used to measure the surface morphology and 2D layer thicknesses.

ASSOCIATED CONTENT

Supporting Information

The Supporting Information is available free of charge at https://pubs.acs.org/doi/10.1021/acsnano.0c02649.

Nonlinear optical responses of $MoTe_2$ and MoS_2; optical microscopy, AFM, and Raman characterizations; and SHG/FWM mapping of few-layer $MoTe_2$ after fs laser irradiation (PDF)

AUTHOR INFORMATION

Corresponding Author

Dawei Li − *Department of Physics and Astronomy, University of Nebraska−Lincoln, Lincoln, Nebraska 68588-0299, United States;* orcid.org/0000-0001-6967-4968; Email: dli8@unl.edu

Authors

Mengmeng Wang − *Laser Micro/Nano Fabrication Laboratory, School of Mechanical Engineering, Beijing Institute of Technology, Beijing 100081, China*

Kun Liu − *School of Optoelectronic Engineering and Instrument Science, Dalian University of Technology, Dalian, Liaoning 116024, China*

Qitong Guo − *Laser Micro/Nano Fabrication Laboratory, School of Mechanical Engineering, Beijing Institute of Technology, Beijing 100081, China*

https://dx.doi.org/10.1021/acsnano.0c02649
ACS Nano XXXX, XXX, XXX−XXX

Sumei Wang − *Laser Micro/Nano Fabrication Laboratory, School of Mechanical Engineering, Beijing Institute of Technology, Beijing 100081, China; Department of Mechanical and Mechatronics Engineering, University of Waterloo, Waterloo, Ontario N2L 3G1, Canada*

Xin Li − *Laser Micro/Nano Fabrication Laboratory, School of Mechanical Engineering, Beijing Institute of Technology, Beijing 100081, China;* orcid.org/0000-0002-4743-5509

Complete contact information is available at: https://pubs.acs.org/10.1021/acsnano.0c02649

Notes

The authors declare no competing financial interest.

ACKNOWLEDGMENTS

The authors gratefully acknowledge the financial support of National Key R&D Program of China (Grant No. 2017YFB1104300), Beijing Municipal Commission of Education (Grant No. KM201910005003), Research Foundation from Ministry of Education of China (Grant No. 6141A02033123), Beijing Natural Science Foundation (Grant No. 3194045), and The Initiative Postdocs Supporting Program (Grant No. BX20180041).

REFERENCES

(1) Choi, W.; Choudhary, N.; Han, G. H.; Park, J.; Akinwande, D.; Lee, Y. H. Recent Development of Two-Dimensional Transition Metal Dichalcogenides and Their Applications. *Mater. Today* **2017**, *20*, 116−130.

(2) Manzeli, S.; Ovchinnikov, D.; Pasquier, D.; Yazyev, O. V.; Kis, A. 2D Transition Metal Dichalcogenides. *Nat. Rev. Mater.* **2017**, *2*, 17033.

(3) Schaibley, J. R.; Yu, H.; Clark, G.; Rivera, P.; Ross, J. S.; Seyler, K. L.; Yao, W.; Xu, X. Valleytronics in 2D Materials. *Nat. Rev. Mater.* **2016**, *1*, 16055.

(4) Li, D.; Huang, X.; Xiao, Z.; Chen, H.; Zhang, L.; Hao, Y.; Song, J.; Shao, D.-F.; Tsymbal, E. Y.; Lu, Y.; Hong, X. Polar Coupling Enabled Nonlinear Optical Filtering at MoS_2/Ferroelectric Heterointerfaces. *Nat. Commun.* **2020**, *11*, 1422.

(5) Mak, K. F.; Shan, J. Photonics and Optoelectronics of 2D Semiconductor Transition Metal Dichalcogenides. *Nat. Photonics* **2016**, *10*, 216−226.

(6) Li, D.; Xiong, W.; Jiang, L.; Xiao, Z.; Golgir, H. R.; Wang, M.; Huang, X.; Zhou, Y.; Lin, Z.; Song, J.; Ducharme, S.; Jiang, L.; Silvain, J. F.; Lu, Y. Multimodal Nonlinear Optical Imaging of MoS_2 and MoS_2-Based van der Waals Heterostructures. *ACS Nano* **2016**, *10*, 3766−3775.

(7) Empante, T. A.; Zhou, Y.; Klee, V.; Nguyen, A. E.; Lu, I.-H.; Valentin, M. D.; Naghibi Alvillar, S. A.; Preciado, E.; Berges, A. J.; Merida, C. S. Chemical Vapor Deposition Growth of Few-Layer $MoTe_2$ in the 2H, 1T′, and 1T Phases: Tunable Properties of $MoTe_2$ Films. *ACS Nano* **2017**, *11*, 900−905.

(8) Cho, S.; Kim, S.; Kim, J. H.; Zhao, J.; Seok, J.; Keum, D. H.; Baik, J.; Choe, D.-H.; Chang, K. J.; Suenaga, K.; Kim, S. W.; Lee, Y. H.; Yang, H. Phase Patterning for Ohmic Homojunction Contact in $MoTe_2$. *Science* **2015**, *349*, 625−628.

(9) Tan, Y.; Luo, F.; Zhu, M.; Xu, X.; Ye, Y.; Li, B.; Wang, G.; Luo, W.; Zheng, X.; Wu, N.; Yu, Y.; Qin, S.; Zhang, X.-A. Controllable 2H-to-1T′ Phase Transition in Few-Layer $MoTe_2$. *Nanoscale* **2018**, *10*, 19964−19971.

(10) Song, S.; Keum, D. H.; Cho, S.; Perello, D.; Kim, Y.; Lee, Y. H. Room Temperature Semiconductor−Metal Transition of $MoTe_2$ Thin Films Engineered by Strain. *Nano Lett.* **2016**, *16*, 188−193.

(11) Hou, W.; Azizimanesh, A.; Sewaket, A.; Peña, T.; Watson, C.; Liu, M.; Askari, H.; Wu, S. M. Strain-Based Room-Temperature Non-Volatile $MoTe_2$ Ferroelectric Phase Change Transistor. *Nat. Nanotechnol.* **2019**, *14*, 668−673.

(12) Huang, H.; Fan, X.; Singh, D. J.; Chen, H.; Jiang, Q.; Zheng, W. Controlling Phase Transition for Single-Layer MTe_2 (M= Mo and W): Modulation of the Potential Barrier under Strain. *Phys. Chem. Chem. Phys.* **2016**, *18*, 4086−4094.

(13) Nan, H.; Jiang, J.; Xiao, S.; Chen, Z.; Luo, Z.; Zhang, L.; Zhang, X.; Qi, H.; Gu, X.; Wang, X.; Ni, Z. Soft Hydrogen Plasma Induced Phase Transition in Monolayer and Few-Layer $MoTe_2$. *Nanotechnology* **2019**, *30*, No. 034004.

(14) Wang, Q.; Chen, J.; Zhang, Y.; Hu, L.; Liu, R.; Cong, C.; Qiu, Z.-J. Precise Layer Control of $MoTe_2$ by Ozone Treatment. *Nanomaterials* **2019**, *9*, 756.

(15) Wang, Y.; Xiao, J.; Zhu, H.; Li, Y.; Alsaid, Y.; Fong, K. Y.; Zhou, Y.; Wang, S.; Shi, W.; Wang, Y.; Zettl, A.; Reed, E. J.; Zhang, X. Structural Phase Transition in Monolayer $MoTe_2$ Driven by Electrostatic Doping. *Nature* **2017**, *550*, 487−491.

(16) Yoo, Y.; DeGregorio, Z. P.; Su, Y.; Koester, S. J.; Johns, J. E. In-Plane 2H-1T′ $MoTe_2$ Homojunctions Synthesized by Flux-Controlled Phase Engineering. *Adv. Mater.* **2017**, *29*, 1605461.

(17) Ma, R.; Zhang, H.; Yoo, Y.; Degregorio, Z. P.; Jin, L.; Golani, P.; Ghasemi Azadani, J.; Low, T.; Johns, J. E.; Bendersky, L. A.; Davydov, A. V.; Koester, S. J. $MoTe_2$ Lateral Homojunction Field-Effect Transistors Fabricated Using Flux-Controlled Phase Engineering. *ACS Nano* **2019**, *13*, 8035−8046.

(18) Yang, L.; Zhang, W.; Li, J.; Cheng, S.; Xie, Z.; Chang, H. Tellurization Velocity-Dependent Metallic−Semiconducting−Metallic Phase Evolution in Chemical Vapor Deposition Growth of Large-Area, Few-Layer $MoTe_2$. *ACS Nano* **2017**, *11*, 1964−1972.

(19) Chen, Z.; Nan, H.; Liu, Z.; Wang, X.; Gu, X.; Xiao, S. Effect of Thermal Conductivity of Substrate on Laser-Induced Phase Transition of $MoTe_2$. *J. Raman Spectrosc.* **2019**, *50*, 755−761.

(20) Yao, Y. L.; Chen, H.; Zhang, W. Time Scale Effects in Laser Material Removal: A Review. *Int. J. Adv. Manuf. Technol.* **2005**, *26*, 598−608.

(21) Jiang, L.; Wang, A.-D.; Li, B.; Cui, T.-H.; Lu, Y.-F. Electrons Dynamics Control by Shaping Femtosecond Laser Pulses in Micro/Nanofabrication: Modeling, Method, Measurement and Application. *Light: Sci. Appl.* **2018**, *7*, 17134.

(22) Phillips, K. C.; Gandhi, H. H.; Mazur, E.; Sundaram, S. K. Ultrafast Laser Processing of Materials: A Review. *Adv. Opt. Photonics* **2015**, *7*, 684−712.

(23) Wang, M.; Jiang, L.; Wang, S.; Guo, Q.; Tian, F.; Chu, Z.; Zhang, J.; Li, X.; Lu, Y. Multiscale Visualization of Colloidal Particle Lens Array Mediated Plasma Dynamics for Dielectric Nanoparticle Enhanced Femtosecond Laser-Induced Breakdown Spectroscopy. *Anal. Chem.* **2019**, *91*, 9952−9961.

(24) Wang, M.; Guo, Q.; Wang, S.; Zhu, W.; Tian, F.; Wei, Y.; Ji, P.; Li, X.; Yang, J. Interference Femtosecond Laser Stamping of Micro-Grating Structures and Time-Resolved Observation of Its Dynamics. *Opt. Express* **2020**, *28*, 18376−18386.

(25) Li, D. W.; Zhou, Y. S.; Huang, X.; Jiang, L.; Silvain, J. F.; Lu, Y. F. *In Situ* Imaging and Control of Layer-By-Layer Femtosecond Laser Thinning of Graphene. *Nanoscale* **2015**, *7*, 3651−3659.

(26) Lin, Z.; Ye, X.; Han, J.; Chen, Q.; Fan, P.; Zhang, H.; Xie, D.; Zhu, H.; Zhong, M. Precise Control of the Number of Layers of Graphene by Picosecond Laser Thinning. *Sci. Rep.* **2015**, *5*, 11662.

(27) An, S.-J.; Kim, Y. H.; Lee, C.; Park, D. Y.; Jeong, M. S. Exfoliation of Transition Metal Dichalcogenides by a High-Power Femtosecond Laser. *Sci. Rep.* **2018**, *8*, 12957.

(28) Pan, Y.; Yang, M.; Li, Y.; Wang, Z.; Zhang, C.; Zhao, Y.; Yao, J.; Wu, Q.; Xu, J. Threshold Dependence of Deep- and Near-Subwavelength Ripples Formation on Natural MoS_2 Induced by Femtosecond Laser. *Sci. Rep.* **2016**, *6*, 19571.

(29) Zuo, P.; Jiang, L.; Li, X.; Tian, M.; Xu, C.; Yuan, Y.; Ran, P.; Li, B.; Lu, Y. Maskless Micro/Nanopatterning and Bipolar Electrical Rectification of MoS_2 Flakes through Femtosecond Laser Direct Writing. *ACS Appl. Mater. Interfaces* **2019**, *11*, 39334−39341.

(30) Huang, M.; Zhao, F.; Cheng, Y.; Xu, N.; Xu, Z. Origin of Laser-Induced Near-Subwavelength Ripples: Interference between Surface Plasmons and Incident Laser. *ACS Nano* **2009**, *3*, 4062−4070.
(31) Li, Y.; Rao, Y.; Mak, K. F.; You, Y.; Wang, S.; Dean, C. R.; Heinz, T. F. Probing Symmetry Properties of Few-Layer MoS_2 and h-BN by Optical Second-Harmonic Generation. *Nano Lett.* **2013**, *13*, 3329−3333.
(32) Cui, Q.; Muniz, R. A.; Sipe, J. E.; Zhao, H. Strong and Anisotropic Third-Harmonic Generation in Monolayer and Multilayer ReS_2. *Phys. Rev. B: Condens. Matter Mater. Phys.* **2017**, *95*, 165406.
(33) Wang, R.; Chien, H.-C.; Kumar, J.; Kumar, N.; Chiu, H.-Y.; Zhao, H. Third-Harmonic Generation in Ultrathin Films of MoS_2. *ACS Appl. Mater. Interfaces* **2014**, *6*, 314−318.
(34) Song, Y.; Tian, R.; Yang, J.; Yin, R.; Zhao, J.; Gan, X. Second Harmonic Generation in Atomically Thin $MoTe_2$. *Adv. Opt. Mater.* **2018**, *6*, 1701334.
(35) Beams, R.; Cançado, L. G.; Krylyuk, S.; Kalish, I.; Kalanyan, B.; Singh, A. K.; Choudhary, K.; Bruma, A.; Vora, P. M.; Tavazza, F.; Davydov, A. V.; Stranick, S. J. Characterization of Few-Layer 1T′ $MoTe_2$ by Polarization-Resolved Second Harmonic Generation and Raman Scattering. *ACS Nano* **2016**, *10*, 9626−9636.
(36) Wang, Y.; Xiao, J.; Yang, S.; Wang, Y.; Zhang, X. Second Harmonic Generation Spectroscopy on Two-Dimensional Materials [Invited]. *Opt. Mater. Express* **2019**, *9*, 1136−1149.
(37) Hsu, W.-T.; Zhao, Z.-A.; Li, L.-J.; Chen, C.-H.; Chiu, M.-H.; Chang, P.-S.; Chou, Y.-C.; Chang, W.-H. Second Harmonic Generation from Artificially Stacked Transition Metal Dichalcogenide Twisted Bilayers. *ACS Nano* **2014**, *8*, 2951−2958.
(38) Hendry, E.; Hale, P. J.; Moger, J.; Savchenko, A. K.; Mikhailov, S. A. Coherent Nonlinear Optical Response of Graphene. *Phys. Rev. Lett.* **2010**, *105*, No. 097401.
(39) Shao, M.; Liang, F.; Yu, H.; Zhang, H. Pushing Periodic-Disorder-Induced Phase Matching into the Deep-Ultraviolet Spectral Region: Theory and Demonstration. *Light: Sci. Appl.* **2020**, *9*, 45.
(40) Wei, D.; Wang, C.; Wang, H.; Hu, X.; Wei, D.; Fang, X.; Zhang, Y.; Wu, D.; Hu, Y.; Li, J. Experimental Demonstration of a Three-Dimensional Lithium Niobate Nonlinear Photonic Crystal. *Nat. Photonics* **2018**, *12*, 596−600.
(41) Yamamoto, M.; Wang, S. T.; Ni, M.; Lin, Y.-F.; Li, S.-L.; Aikawa, S.; Jian, W.-B.; Ueno, K.; Wakabayashi, K.; Tsukagoshi, K. Strong Enhancement of Raman Scattering from a Bulk-Inactive Vibrational Mode in Few-Layer $MoTe_2$. *ACS Nano* **2014**, *8*, 3895−3903.
(42) Ben-Yakar, A.; Harkin, A.; Ashmore, J.; Byer, R. L.; Stone, H. A. Thermal and Fluid Processes of a Thin Melt Zone During Femtosecond Laser Ablation of Glass: The Formation of Rims by Single Laser Pulses. *J. Phys. D: Appl. Phys.* **2007**, *40*, 1447−1459.
(43) Pan, S.; Ceballos, F.; Bellus, M. Z.; Zereshki, P.; Zhao, H. Ultrafast Charge Transfer between $MoTe_2$ and MoS_2 Monolayers. *2D Mater.* **2017**, *4*, No. 015033.
(44) Peng, B.; Zhang, H.; Chen, W.; Hou, B.; Qiu, Z.-J.; Shao, H.; Zhu, H.; Monserrat, B.; Fu, D.; Weng, H.; Soukoulis, C. M. Sub-Picosecond Photo-Induced Displacive Phase Transition in Two-Dimensional $MoTe_2$. *npj 2D Mater. Appl.* **2020**, *4*, 14.
(45) Kolobov, A. V.; Fons, P.; Tominaga, J. Electronic Excitation-Induced Semiconductor-To-Metal Transition in Monolayer $MoTe_2$. *Phys. Rev. B: Condens. Matter Mater. Phys.* **2016**, *94*, No. 094114.
(46) Krishnamoorthy, A.; Bassman, L.; Kalia, R. K.; Nakano, A.; Shimojo, F.; Vashishta, P. Semiconductor−Metal Structural Phase Transformation in $MoTe_2$ Monolayers by Electronic Excitation. *Nanoscale* **2018**, *10*, 2742−2747.
(47) Yuan, S.; Luo, X.; Chan, H. L.; Xiao, C.; Dai, Y.; Xie, M.; Hao, J. Room-Temperature Ferroelectricity in $MoTe_2$ down to the Atomic Monolayer Limit. *Nat. Commun.* **2019**, *10*, 1775.
(48) Bonse, J.; Höhm, S.; Kirner, S. V.; Rosenfeld, A.; Krüger, J. Laser-Induced Periodic Surface Structures - A Scientific Evergreen. *IEEE J. Sel. Top. Quantum Electron.* **2017**, *23*, 9000615.
(49) Reif, J.; Varlamova, O.; Varlamov, S.; Bestehorn, M. The Role of Asymmetric Excitation in Self-Organized Nanostructure Formation upon Femtosecond Laser Ablation. *Appl. Phys. A: Mater. Sci. Process.* **2011**, *104*, 969−973.
(50) Sedao, X.; Shugaev, M. V.; Wu, C.; Douillard, T.; Esnouf, C.; Maurice, C.; Reynaud, S.; Pigeon, F.; Garrelie, F.; Zhigilei, L. V.; Colombier, J.-P. Growth Twinning and Generation of High-Frequency Surface Nanostructures in Ultrafast Laser-Induced Transient Melting and Resolidification. *ACS Nano* **2016**, *10*, 6995−7007.
(51) Straub, M.; Afshar, M.; Feili, D.; Seidel, H.; König, K. Surface Plasmon Polariton Model of High-Spatial Frequency Laser-Induced Periodic Surface Structure Generation in Silicon. *J. Appl. Phys.* **2012**, *111*, 124315.
(52) Dhar, S.; Barman, A. R.; Ni, G. X.; Wang, X.; Xu, X. F.; Zheng, Y.; Tripathy, S.; Ariando; Rusydi, A.; Loh, K. P.; Rubhausen, M.; Neto, A. H. C.; Özyilmaz, B.; Venkatesan, T. A New Route to Graphene Layers by Selective Laser Ablation. *AIP Adv.* **2011**, *1*, No. 022109.
(53) Nagareddy, V. K.; Octon, T. J.; Townsend, N. J.; Russo, S.; Craciun, M. F.; Wright, C. D. Humidity-Controlled Ultralow Power Layer-By-Layer Thinning, Nanopatterning and Bandgap Engineering of $MoTe_2$. *Adv. Funct. Mater.* **2018**, *28*, 1804434.
(54) Ruppert, C.; Aslan, O. B.; Heinz, T. F. Optical Properties and Band Gap of Single- and Few-Layer $MoTe_2$ Crystals. *Nano Lett.* **2014**, *14*, 6231−6236.
(55) Kollipara, P. S.; Li, J.; Zheng, Y. Optical Patterning of Two-Dimensional Materials. *Research* **2020**, *2020*, 6581250.

https://dx.doi.org/10.1021/acsnano.0c02649
ACS Nano XXXX, XXX, XXX−XXX

View publication stats